Turbulent Schmidt Number Measurements in a Polymer Drag-Reduced Turbulent Boundary Layer

V. S. R. Somandepalli*, Y. X. Hou* & M. G. Mungal*[#]
*Mechanical Engineering Department,
Stanford University, Stanford, CA 94305, USA
[#]Dean, School of Engineering,
Santa Clara University, Santa Clara, CA 95053, USA
mungal@stanford.edu, mgmungal@scu.edu

ABSTRACT

In this work we investigate zero pressure gradient turbulent boundary layer (TBL) drag reduction (DR) by polymer injected from a single upstream slot using simultaneous Particle Image Velocimetry (PIV) and Planar Laser Induced Fluorescence (PLIF). The data allow the computation of the turbulent fluxes in the streamwise and wall-normal directions. The results show a suppression of fluxes at positions closer to the injection slot where the drag reduction is highest, with a recovery towards an undisturbed boundary layer with downstream distance. The turbulent Schmidt number is computed and shown to be as high as 5 at high drag reduction and reducing towards unity as drag reduction decreases.

INTRODUCTION

The addition of dilute polymer solutions to turbulent wall bounded flows can cause a significant reduction in the skin friction drag. This drag reducing effect of polymers, called the Toms effect (1948), has been well known for more than 50 years. This reduction in skin friction, if applied to practical systems optimally, can lead to significant savings in fuel and travel time of ships and submarines.

The reduction of the skin friction due to polymer addition causes modification of the mean velocity profile (Virk 1975), changes in the turbulence structure and vorticity in the flow and leads to a redistribution of the stresses in the fluid. This interaction of the polymer solution with the near wall turbulence and its subsequent modification of the self sustaining mechanism of near wall turbulence (Jimenez & Pinelli, 1999) are profoundly important to the understanding of the mechanism of polymer DR. Past studies (e.g. Oldaker & Tiederman 1977, McComb & Rabie 1982, Warholic *et al.* 2001, Ptasinski *et al.* 2001, 2003) to understand the physics of DR due to polymers have been mainly concentrated on cases with a <u>homogeneous</u> distribution of polymers in a pipe or channel flow, i.e., an ocean of polymer flowing through a pipe/channel. The present work instead examines the TBL case, with slot injection of polymer following Wu & Tulin (1972), Fruman & Tulin (1976), Vdovin, & Smol'yakov (1981), Tiederman *et al.,* (1985), Fontaine *et al.* (1992), Petrie & Fontaine (1996), Petrie *et al.* (2003), L'vov *et al.* (2004), but focuses on measurements of the turbulent fluxes which requires simultaneous measurement of the velocity and concentration fields. The present work is a continuation of a larger effort on TBL DR described by White *et al.*

(2004) and Hou *et al.* (2008). White & Mungal (2008) provide a recent overview of polymer DR in a TBL.

EXPERIMENTAL DETAILS

The experiments were conducted in a constant head closed circuit water tunnel maintained at a ZPG condition, with a detailed description of the water tunnel facility given in White *et al.* (2004). The test section had a cross section of 0.36 m in span and 0.13 m in height with a length of 3.66 m. The walls of the tunnel were constructed from acrylic to provide full optical access to the top wall which served as the test surface. The flow inlet velocity was maintained constant at 0.5 m/s while the temperature was maintained at a constant value of 18 ± 0.2 °C. The leading edge of the test wall was a half ellipse with major to minor axis ratio of 16. A 0.6 mm diameter rod glued 25.4 mm downstream of the leading edge was used to trip the boundary layer and make it turbulent.

Table 1 Newtonian TBL parameters. x = distance from leading edge; δ = boundary layer thickness at u/U = 99%; θ = momentum thickness, and Re_θ = Reynolds number based on momentum thickness = $U\theta/v$.

Typical TBL parameters for $U = 0.5$ m/s					
Position	x (mm)	x^+ (based on local u_τ)	δ (mm)	θ (mm)	Re_θ
x02	343	7690	13	1.6	730
Inj. slot	483	10640	15	1.8	840
x06	597	12900	17	2.1	970
x1	737	15320	20	2.5	1150
x2	1168	23320	27	3.5	1620
x3	1651	31310	35	4.5	2060
x4	2108	39400	42	5.2	2380

Table 1 gives a comprehensive listing of the boundary layer parameters at each of the measurement stations. There are six measurement positions on the flat plate designated *x02*, *x06*, *x1*, *x2*, *x3* and *x4* as shown in Fig. 1. The injection slot was located between position *x02* and *x06* and was 483 mm downstream of the plate's leading edge. For a purely Newtonian boundary layer with a freestream velocity of 0.5 m/s, the boundary layer thickness varied from 13 mm at position *x02* to 42 mm at position *x4*.

The polymer used was poly-ethylene oxide (PEO) WSR-301 from Dow Chemical Co. The mean molecular

weight, based on the manufacturer's specification sheet, was ~4 million. The polymer solution was prepared by directly mixing the polymer powder with water which was filtered by a carbon filter to remove all contaminants and residual chlorine. After all polymer powder had been added to the solution, it was gently stirred for several hours periodically. The solutions were then allowed to stand for at least 20 hours to homogenize and allow degassing.
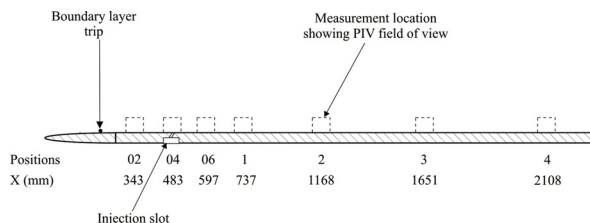

Figure 1: Schematic showing boundary layer flat plate, measurement locations and their distances (not to scale).

Polymer concentrations of 100, 250, 500, 1000 and 2000 wppm were investigated. The polymer solution was injected into the boundary layer through an injection slot by pressurizing its holding container slightly above the tunnel pressure ($\sim$ 41 kPa) with compressed air. The single injection slot was inclined at 30° to the flat plate and had dimensions of 0.45 mm width, 10 mm flow entrance length and 310 mm in span.

The injection rate of polymer is denoted by the ratio Q_i/Q_s, where Q_i is the flow rate of the injected fluid; Q_s (= 67.3v) is the volume flow rate of water in the viscous sublayer (defined by the sublayer edge at $y^+ = 11.6$) of the boundary layer and is independent of velocity. In order to minimize the disturbance of the injected flow on the boundary layer, Q_i should be smaller or on the same order as Q_s (Wu & Tulin 1972, Walker & Tiederman 1990, Fontaine *et al.* 1992). The typical injection rate in the current experiment was about 0.77 so that the injection disturbance was small. The injector width in plus units is 11 and is thus within the sublayer. The injection velocity is high at 23% of the freestream velocity. However, as discussed previously by Hou *et al.,* (2008), the overall disturbance to the flow due to injection is quite small and can be neglected.

Flow diagnostics

Particle Imaging Velocimetry (PIV) was used to measure velocity and velocity statistics in these experiments. The PIV system used a Peltier cooled 12 bit CCD camera with a resolution of 1280 × 1024 pixels, a dual head - pulsed Nd:YAG laser operating at 532nm, and appropriate sheet forming optics. A 532nm narrowband filter was used in conjunction with the camera optics to allow only the laser light scattered by the tracer particles into the camera. The flow was naturally seeded with residual dust particles in the water of size less than 10 microns. All particles above this size were removed by a series of filters before the water entered the tunnel system. The natural seeding by dust in the water gave consistent and good particle images and hence all PIV measurements were performed with this. The PIV processing algorithms used a multi-pass iterative scheme starting with a cross-correlation window box size of 64 × 64 pixels and a final pass at 32 × 32 pixels with 50% overlap between adjacent correlation regions. The spatial resolution of the camera was 13.6 μm per pixel with an effective field of view of 17.4 mm × 13.9 mm. At this resolution, the smallest scale resolved by the PIV camera was 435 μm. At a fixed streamwise location, PIV images were obtained across the full thickness of the boundary layer in the *x-y* plane (the plane perpendicular to the flat plate and in line with the flow direction). Closer to the leading edge, a single PIV image spanned the entire thickness of the boundary layer; while further downstream, as the thickness of the boundary layer increased, multiple PIV images in the wall normal direction were needed to span the entire thickness of the boundary layer. One thousand image pairs were acquired at each streamwise location and averaged to give the velocity profiles and statistics. A detailed and complete description of the PIV system and the algorithms used is presented in Hou *et al.* (2008).

PLIF was used to quantitatively measure the concentrations on the injected polymer solution in the boundary layer. The PLIF measurement system was piggybacked on the existing PIV setup to simplify the optics and also to ensure high quality of the data obtained. The PIV system used a Nd:YAG laser at 532 nm and it was desirable to use to use the same laser for the PLIF measurements too. Several members of the Rhodamine family of dyes are well suited to be used with 532nm excitation. However, a majority of these dyes are considered carcinogenic and toxic and cannot be used. Rhodamine-WT, a member of this species is well suited for use in these experiments as it is non-toxic and non-carcinogenic – it is used in tracking and measuring various parameters in river water – and it fluoresces under the action of 532nm light and the emitted light (Putorti *et al.* 2003) used for concentration measurements here is well separated from the excitation wavelength and can, hence, be filtered easily. For the experiments presented here, a Schott glass filter, OG-550, from CVI Laser Inc. was used to filter out the laser excitation light. The emitted light was captured using the same 12 bit CCD cameras used for the PIV system described above.

Combined PIV and PLIF measurements

The PLIF camera was situated on the opposite side of the tunnel with respect to the PIV camera. As a result, the region imaged by the PLIF camera was laterally inverted compared to the image from the PIV image. The cameras were situated such that the regions imaged by each camera had the maximum overlap with the other. The PLIF camera lens was operated at a slightly lower magnification than the PIV lens (ratio of PLIF image size: PIV image size = 1.04:1) so that the PLIF camera saw a slightly larger field of view and completely enclosed the region seen by the PIV camera. By imaging a static target with a fiducial mark, the exact region viewed by both cameras was recorded. Subsequently, the PLIF image orientation is mapped, by mirroring along the vertical, to the same orientation as the PIV image. Linear, rotational and angular distortions in the images from the PLIF camera were corrected by using standard image processing and rotation algorithms. This

gross matching procedure gives a mapping between the PLIF and the PIV camera images for each measurement location. Based on this map, the appropriate scaling for the PLIF images with respect to the PIV images were calculated and used in all subsequent computations to match individual vectors with the polymer concentration at its location.

As part of the PIV measurements, 1000 image pairs are obtained at each measurement location in every experiment. Correspondingly, 1000 PLIF images are also simultaneously obtained. This is done at all five measurement stations and the data is processed as a batch at the end of the experiment to obtain the PIV vectors. The PIV vectors are processed to obtain fluctuating velocity vector frames by subtracting the mean velocity profiles from each raw velocity vector frame. Each of these fluctuation velocity vector frames consists of a 64 x 80 array of velocity vectors. The PLIF images give the concentration of the injected polymer at every point (pixel) on the image. This data has to be binned appropriately so that the velocity fluctuation vector can then be correlated with a single value of the polymer concentration at its location.

The location of each velocity vector in the PIV vector frame is known in terms of an x and y array of pixels. Using the calibration of the PIV camera, these pixels are converted to a physical location relative to the boundary layer flat plate and one fixed edge of the PIV image that is perpendicular to the flat plate. This physical location is then located on the PLIF image using the mapping obtained by the image matching described above. Using the camera scales for the PLIF camera, this physical location is converted into a two dimensional pixel location on the PLIF image. An average polymer concentration at this location is then calculated by binning a square region of size 15 x 15 pixels around this location to obtain an average value of the polymer concentration at this location. This algorithm is executed for each of the 64 x 80 vectors in each PIV vector frame to give a frame containing 64 x 80 values of the polymer concentration for each PLIF image. This entire process is then repeated for the 1000 images that are obtained at each measurement location in every experiment. The concentration data frames are stored for further analysis.

RESULTS

Our work is aimed at providing fundamental understanding of the changes to a turbulent boundary layer at conditions ranging from zero drag reduction (DR) to maximum drag reduction (MDR). A previously developed technique - the (1-y/δ) fit to the total shear stress profile (Hou *et al.* 2006) - has been used to evaluate the wall skin friction and hence the drag reduction. The streamwise evolution of drag reduction magnitude is used to divide the flow into three regions: development region, steady-state region and depletion region. Results for mean velocity profiles, velocity fluctuations and Reynolds stresses are in good agreement with previously published data (Warholic *et al.* 1999) with detailed comparisons provided in Hou *et al.* (2008). Results for the mean and fluctuating concentration profiles are also in good agreement with previously published results (Fontaine *et al.* 1992) and can be found in Somandepalli *et al.* (2008a, b)

Flow Images

Figure 2 shows examples of the dramatic change to the flow which occurs with polymer injection from a single upstream slot. Here, the dye which marks the injected polymer solution, is seen to remain in higher concentrations and is less diffused across the boundary layer implying a suppression of turbulent activity with polymer injection. These images suggest a reduced level of turbulent activity which impacts the transport of polymer in the BL.
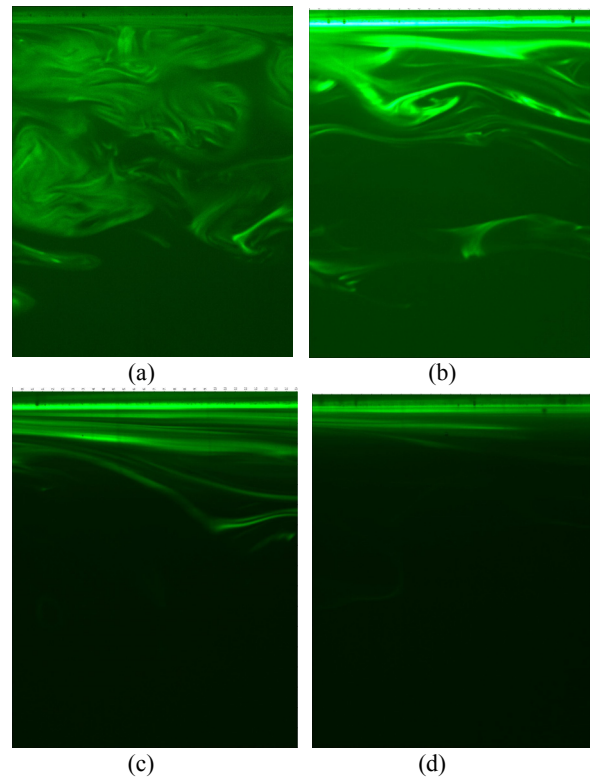

(a)   (b)

(c)   (d)

Figure 2: Typical PLIF images for the (a) water case, (b) 100 ppm, (c) 250 ppm, (d) 500 ppm polymer case at position *x1*, 73 cm downstream of the injection slot. U = 0.5 m/s. In each case, image size is 17.5mm x 14.3mm (H x W). Top edge is wall location. Boundary layer is 20 mm thick. Flow is left to right.

Flux Measurements

Concentration fluctuation fields corresponding to individual PIV vector frames are calculated by subtracting the local value of mean concentration from the concentration field frames. From these, concentration flux fields containing information about both the streamwise and wall normal flux, at each vector location are obtained by multiplying the concentration fluctuations with the velocity fluctuations at that location.

$$cu_k(i, j) = c_k(i, j)u_k(i, j)$$

where $cu_k(i,j)$ is the concentration flux field, $c_k(i,j)$ is the concentration fluctuation field and $u_k(i,j)$ is the velocity field in the kth frame referenced. These concentration flux fields are ensemble averaged over the 1000 frames captured to give a single frame which is then line averaged over the 64 columns to give a single concentration flux profile for

both the streamwise and wall normal flux at each measurement location,

$$< cu(i,j) > = \frac{1}{1000} \sum_{k=1}^{1000} cu_k(i,j)$$

$$< cu > = \frac{1}{64} \sum_{j=1}^{64} cu(i,j)$$

where the indices i, j refer to the row and column number of the quantities in each frame, k. These concentration flux profiles are used to calculate higher order turbulence quantities such as turbulent fluxes, turbulent Schmidt numbers and the total polymer flux budget in the boundary layer.
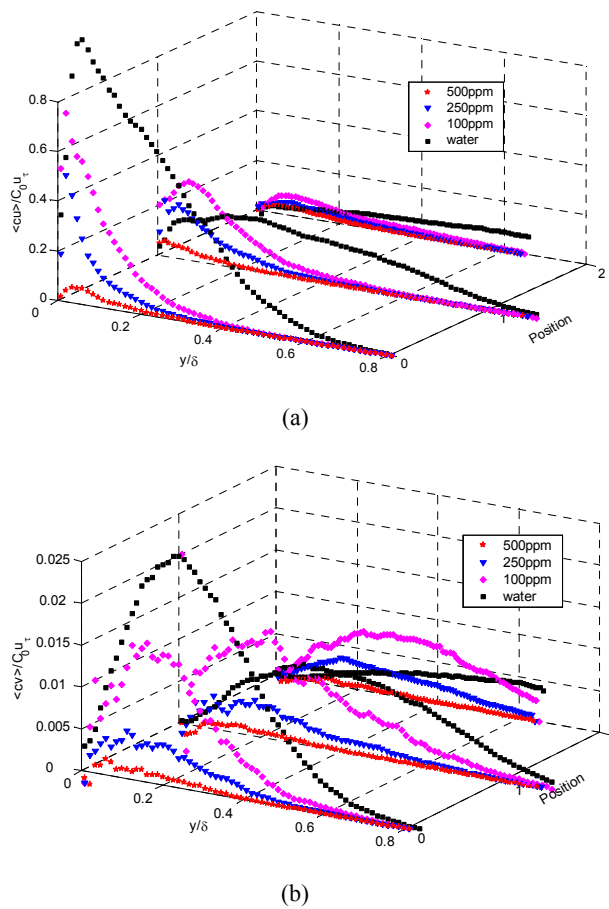

(a)

(b)

Figure 3. Evolution of turbulent fluxes along the flat plate for the water injection and polymer injection cases. (a) shows the streamwise fluxes and (b) the wall-normal fluxes. Both quantities normalized by the initial injection concentration and friction velocity.

Figure 3 shows the evolution of turbulent fluxes along the flat plate for the water case and polymer injection cases. Figure 3(a) shows the streamwise fluxes while Fig. 3(b) shows the wall-normal fluxes. Both quantities are normalized by the initial injection concentration and friction velocity. The four cases shown are: water (i.e. no polymer present), 100 pppm injection, 250 ppm injection and 500 ppm injection of WSR 301 PEO polymer. The clear suppression of the turbulent fluxes is seen in both figures and is consistent with the flow visualization images shown in Fig. 2.

It is instructive to study how the streamwise fluxes, in the different concentrations tested, evolve across several measurement stations relative to each other (Fig. 3a). The profiles show clearly how the concentration of the injected solution influences the decay rates of the streamwise fluxes. The 100ppmw case, decays rapidly from position 06 to 2, whereas the 500ppmw case, does not show any significant decay of the streamwise flux between the same 2 positions. The 250ppmw case, as expected, falls between the two extremes comparatively. The location of the peaks of the profiles also can be compared in the same graph. As the concentration of the injected solution increases, the peaks in the flux profiles remain closer to the wall as the distance from injection increases.

The evolution of the wall normal fluxes along the flat plate, for the different concentrations tested, relative to each other is shown in Fig. 3b. As can be seen from the graph, the 100ppmw case, decays the fastest among the three cases, with the peak magnitude dropping significantly compared to the other cases. The movement away from the wall, of the peak in the wall normal flux profile, is also very clearly evident in this case. The 250ppmw case shows a smaller decay rate along the flat plate. The 500ppmw case, with its very low flux magnitudes, shows the least movement, both in terms of change in magnitude and also the location of the peak of the profile. A more detailed discussion of the fluxes is provided in Somandepalli *et al*. (2008b).

Turbulent Schmidt Number

The turbulent Schmidt number (Sc_T), is the ratio of the momentum eddy diffusivity to the concentration eddy diffusivity, and is defined as

$$Sc_T = \frac{\overline{uv}(dC/dy)}{\overline{cv}(dU/dy)}$$

where $\overline{uv}$ is the Reynolds shear stress, $\overline{cv}$ the turbulent wall-normal flux, dC/dy the gradient of the mean concentration and dU/dy the gradient of the mean velocity in the flow. The turbulent Schmidt number is a measure of the relative intensities of the turbulent diffusivities of momentum and concentration (mass) in a flow. The gradients of the mean velocity and the mean concentration are obtained by differentiating the mean velocity and concentration profiles, respectively, using a second order central difference scheme. The differentiation is an inherently noisy process because the derivatives accentuate the noise in the signal. It is also necessary to use various curvefits to the $\overline{cv}$ flux to minimize noise.

Figure 4 shows examples of Sc_T for the water case and 250 ppm polymer injection. In Fig. 4a, the turbulent Schmidt number profiles at all locations are relatively flat with a magnitude of unity over a large portion of the boundary layer. The measurements at position 06 and 1, very clearly show this expected magnitude. Positions 2 and 3 profiles are a little noisier, especially close to the wall and in the free stream. These profiles also show a peak in the turbulent Schmidt numbers close to the wall. This peak and the increasing noise are a numerical artifact of the errors associated with the numerical differentiation used to calculate the gradient of the mean concentration – a quantity that has low signal to noise at these downstream locations

due to turbulent dispersion and mixing away of the injected dye.

The Sc_T profiles obtained in the 250ppmw polymer solution injection case are shown in Fig. 4b. At position 06, the average Sc_T estimated is 3.1 and is higher than the Sc_T obtained at the same position for the 100ppmw case, but less than the 500ppmw case. At position 1, this value decreases to 2.4 and at position 2, it is estimated to be about 1.8. The Sc_T values estimated at position 3 are similar to those obtained at position 2. The Sc_T values estimated in the 250ppmw case are higher than the values estimated for the 100ppmw case at the corresponding locations, but less than the 500ppmw case. This is indicative of the polymer action being more effective in the 500ppmw case followed by the 250ppmw case followed by the 100ppmw case, and consistent with the visualization images of Fig. 2
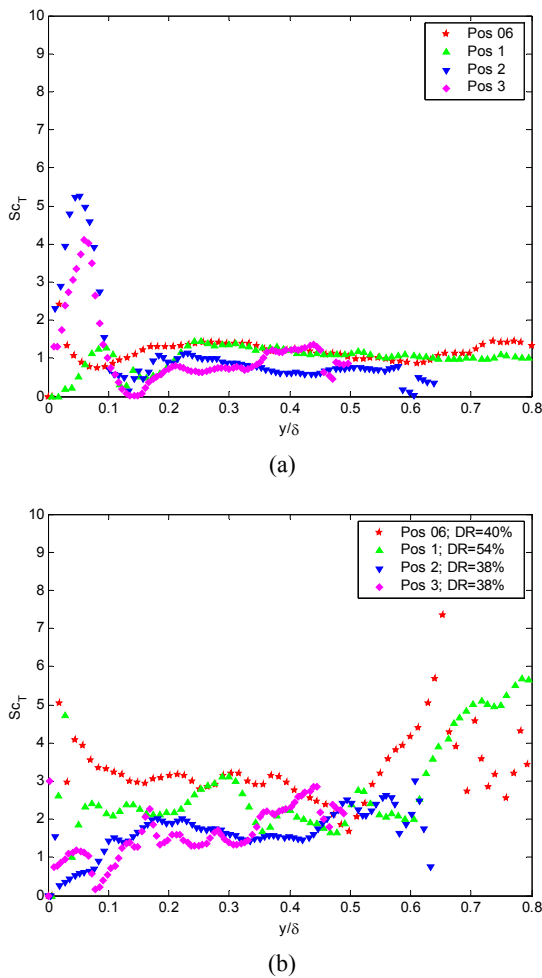

(a)

(b)

Figure 4. Turbulent Schmidt number profiles calculated at each measurement location along the flat plate for (a) water, and (b) 250ppm polymer injection case. Positions are labeled sequentially as 06, 1, 2, 3 with position 06 being closest to the polymer injection slot.

Combining the results from all the experiments presented here gives an overall idea of the drag reduction due to the injection of dilute polymer solutions. The turbulent Schmidt number, Sc_T, combines both the velocity

statistics and the concentration statistics into a single quantity. The variation of Sc_T with drag reduction, as seen from the various experiments presented here, is shown in Fig. 5 (where the DR is estimated using the $(1-y/\delta)$ fit to the total shear stress profile of Hou *et al.,* 2006). In this figure, the Sc_T estimated at a location on the flat plate is plotted against the DR observed at that location, for all measurement locations and experiments performed. Also shown in the plot is a line that approximates the trend obtained from the data plotted. On the lower end of the DR scale, the Sc_T values asymptote to a value close to 1, as is expected for a purely Newtonian flow. As DR increases, the turbulent Schmidt number increases, with a DR of 70% corresponding to an Sc_T of approximately 4.5. At higher drag reductions, based on the increased slope of the trend line, the rate of change of DR is lower for a given change in the Sc_T compared to that at low drag reductions. The scatter noticed in the graph is relatively high, especially in the high DR region and this is most likely due to the fact that the flow can be in the developing, steady state and depletion regimes of the drag reduction state. There is also, likely, a contribution due to the experimental errors and the curve fits used to estimate the Sc_T for the cases tested. We believe that the data shown here can also be used to validate models for simulating polymer DR and can help in formulating new models that better capture the physics of inhomogeneous polymer DR (e.g. Gupta *et al.*, 2005).
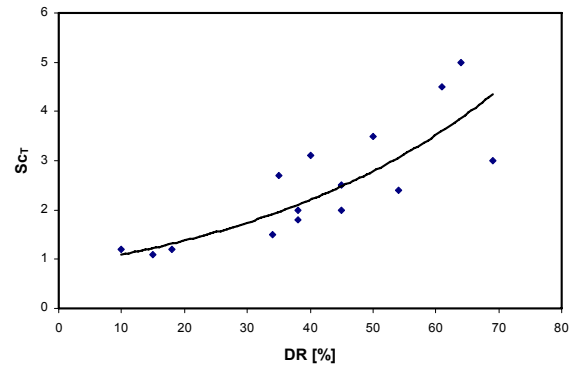

Figure 5: Variation of turbulent Schmidt number with drag reduction observed. Data points from all the experiments presented are plotted together. Also shown is a line approximating the observed trend in the Schmidt number increase with drag reduction.

CONCLUSIONS

In this work we investigate zero pressure gradient turbulent boundary layer (TBL) drag reduction (DR) by polymer injected from a single upstream slot using simultaneous Particle Image Velocimetry (PIV) and Planar Laser Induced Fluorescence (PLIF). The data allow the computation of the turbulent fluxes in the streamwise and wall-normal directions and provide a quantitative measure of the polymer effects on near wall turbulence with emphasis upon the turbulent Schmidt number – an area which has received limited attention in the past.

The flow visualization results show a reduction in turbulent activity at high DR. The quantitative results show a suppression of fluxes at positions closer to the injection slot where the drag reduction is highest, with a recovery

towards an undisturbed boundary layer with downstream distance as the effect of the polymer diminishes. The turbulent Schmidt number is computed and shown to be as high as 5 at high drag reduction and reducing towards unity as the polymer effect and drag reduction decrease, as would be expected. The data provided here can be used for improved understanding of polymer induced DR and as a target for numerical simulations of the DR phenomenon (e.g. Dimitropoulos *et al.* 2005, Dubief *et al.* 2005).

REFERENCES

Dimitropoulos, C. D., Dubief, Y., Shaqfeh, E. S. G., Moin, P. and Lele, S. K., 2005, Direct numerical simulation of polymer-induced drag reduction in turbulent boundary layer flow, *Phys. Fluids*, 17, 011705.

Dubief, Y., Terrapon, V. E., White, C. M., Shaqfeh, E. S. G., Moin, P. and Lele, S. K., 2005, New answers on the interaction between polymers and vortices in turbulent flows, *Flow, Turb. and Comb.* 74, 311-329.

Fontaine, A. A., Petrie, H. L. & Brungart, T. A., 1992, Velocity profile statistics in a turbulent boundary layer with slot-injected polymer, *J. Fluid Mech.*, 56, 559-575.

Fruman, D. H., & Tulin, M. P., 1976, Diffusion of a tangential drag reducing polymer injection of a flat plate at high Reynolds numbers. *J. Ship Res.,* 20, 171-180.

Gupta, V. K., Sureshkumar, R. & Khomami, B., 2005, Passive scalar transport in polymer drag-reduced turbulent channel flow, *AIChE J.*, 51 (7), 1938-1950.

Hou, Y. X., Somandepalli, V. S. R. & Mungal, M. G., 2006, A technique to determine total shear stress and polymer stress profiles in drag reduced boundary layer flows, *Exp. Fluids*, 40, 589-600.

Hou, Y. X., Somandepalli, V. S. R. & Mungal, M. G., 2008, Streamwise development of turbulent boundary layer drag reduction with polymer injection, *J. Fluid Mech.,* 597, 31-66; with correction, 601, 443 (2008).

Jimenez, J. & Pinelli, A., 1999, The autonomous cycle of near-wall turbulence, *J. Fluid Mech.*, 389, 335-359.

L'vov, V. S., Pomyalov, A., Procaccia & I., Tiberkevich, V., 2004, Drag reduction by polymers in wall bounded turbulence, *Phys. Rev. Lett.,* 68, 046308.

McComb, W. D. & Rabie, L. H., 1982, Local drag reduction due to injection of polymer solution into turbulent flow in a pipe. Part 1: dependence on local polymer concentration; and Part II: laser Doppler measurements of turbulence structure. *AIChE Journal.* 28, 547–565.

Oldaker, D. K. & Tiederman, W. G., 1977, Structure of the turbulent boundary layer in drag reducing pipe flow, *Phys. Fluids*, 20, 133-144.

Petrie, H. L. & Fontaine, A. A., 1996, Comparison of turbulent boundary layer modification with slot-injected and homogeneous drag-reducing polymer solutions, *ASME Fluids Eng. Div. Conf.* 237, 205-210.

Petrie, H. L., Deutsch, S., Brungart, T. A. & Fontaine, A. A., 2003, Polymer drag reduction with surface roughness in flat-plate turbulent boundary layer flow, *Exp. Fluids*, 35, 8-23.

Ptasinski, P. K., Boersma, B. J., Nieuwstadt, F. T. M., Hulsen, M. A., Brule, B. H. A. A. V. D. & Hunt, J. C. R., 2003, Turbulent channel flow maximum drag reduction: simulations, experiments and mechanisms, *J. Fluid Mech.*, 490, 251-291.

Ptasinski, P. K., Nieuwstadt, F. T. M., Brule, B. H. A. A. V. D. & Hulsen, M. A., 2001, Experiments in turbulent pipe flow with polymer additives at maximum drag reduction, *Flow, Turb. and Comb.*, 66, 159-182.

Somandepalli, V. S. R., Hou, Y. X. & Mungal, M. G., 2008a, Visualization of Drag Reduced Boundary Layer Flows with Polymer Injection, 13th International Symposium on Flow Visualization*,* July 1-4, 2008, Nice, France.

Somandepalli, V. S. R., Hou, Y. X. & Mungal, M. G. 2008b, Concentration Flux Measurements in a Polymer Drag-Reduced Turbulent Boundary Layer, submitted to *J. Fluid Mech.*

Tiederman, W. G., Luchik, T. S. & Bogard, D. G., 1985, Wall layer structure and drag reduction. *J. Fluid Mech.* 156, 419-437.

Toms, B., 1948, Observation on the flow of linear polymer solutions through straight tubes at large Reynolds numbers, *Proc. Intl. Rheological Congress*, 2, 135-141.

Virk, P. S., 1975, Drag reduction fundamentals, *AIChE J.*, 21, 625.

Virk, P. S., Merril, E. W., Mickley, H. S., Smith, K. A. & Mollo-Christensen, E., 1967, The Toms phenomenon - turbulent pipe flow of dilute polymer solutions, *J. Fluid Mech.*, 30, 305-328.

Vdovin, A. V. & Smol'yakov, A. V., 1981, Turbulent diffusion of polymers in a boundary layer. *Zh. Prikl. Mekh. Tekh. Fiz.* 4, 98-104 (transl. in UDC532.526 (1982) 526-531, Plenum).

Walker, D. T. & Tiederman, W. G., 1990, Turbulent structure in a channel flow with polymer injection at the wall, *J. Fluid Mech.*, 218, 377-403.

Warholic, M. D., Massah, H. & Hanratty, T. J., 1999, Influence of drag-reducing polymers on turbulence: effects of Reynolds number, concentration and mixing, *Exp. Fluids*, 27, 461-472.

Warholic, M. D., Heist, D. K., Katcher, M. & Hanratty, T. J., 2001, A study with particle image velocimetry of the influence of drag reducing polymers on the structure of turbulence, *Exp. Fluids*, 31, 474-483.

White, C. M. & Mungal, M. G., 2008, Mechanics and Prediction of Turbulent Drag Reduction with Polymer Additives, *Ann. Rev. Fluid Mech.*, 40, 235–256.

White, C. M., Somandepalli, V. S. R. & Mungal, M. G., 2004, The turbulence structure of drag reduced boundary layer flow, *Exp. Fluids*, 36, 62-69.

Wu, J. & Tulin, M. P., 1972, Drag reduction by ejecting additive solutions into a pure water boundary layer. *Trans. ASME D: J. Basic Engng* 94, 749-755.